

Search on a Fractal Lattice using a Quantum Random Walk

Apoorva Patel^{1,2,*} and K.S. Raghunathan^{1,†}

¹Centre for High Energy Physics, Indian Institute of Science, Bangalore-560012, India

²Supercomputer Education and Research Centre, Indian Institute of Science, Bangalore-560012, India

(Dated: October 29, 2018)

The spatial search problem on regular lattice structures in integer number of dimensions $d \geq 2$ has been studied extensively, using both coined and coinless quantum walks. The relativistic Dirac operator has been a crucial ingredient in these studies. Here we investigate the spatial search problem on fractals of non-integer dimensions. Although the Dirac operator cannot be defined on a fractal, we construct the quantum walk on a fractal using the flip-flop operator that incorporates a Klein-Gordon mode. We find that the scaling behavior of the spatial search is determined by the spectral (and not the fractal) dimension. Our numerical results have been obtained on the well-known Sierpinski gaskets in two and three dimensions.

PACS numbers: 03.67.Ac

I. INTRODUCTION

The spatial search problem is to find a marked object from an unsorted database of size N spread over distinct locations, with the restriction that one can proceed from any location to only its neighbors while inspecting the objects. Classical algorithms for the unsorted database search can do no better than inspect one location after another, and so are $O(N)$. On the other hand, quantum algorithms can do better by working with a superposition of states. The quantum spatial search problem has been studied extensively in recent years, in a variety of geometries ranging from a single hypercube to regular lattices in various integer dimensions (see for example, Refs. [1–7]). These investigations used local translationally invariant quantum walk operators [8, 9], arising from relativistic quantum mechanics in some form, to obtain their results. Here we investigate the spatial search on a fractal lattice, which has neither a translational symmetry nor a straightforward structure to implement the relativistic Dirac operator. The non-integral value of the fractal dimension also lets us explore the dependence of the spatial search on the geometry of space in more generality.

Our algorithmic strategy for the quantum search is to construct a Hamiltonian evolution, whereby the kinetic term diffuses the amplitude distribution all over the space and the potential term attracts the amplitude distribution toward the marked vertex [10]. In its discrete form, the kinetic term is realized as the quantum walk operator W , explicitly defined in Section III. A relativistic walk provides the fastest diffusion, and is expected to produce the quickest search. The best potential term is the one that provides maximum contrast between the marked vertex and the rest. In its discrete form, it is the

binary oracle. Choosing the origin as the marked vertex,

$$\begin{aligned} V &= V_0 \delta_{\vec{x},0}, \quad e^{-iV_0\tau} = -1 \\ \implies R &= e^{-iV\tau} = I - 2|\vec{0}\rangle\langle\vec{0}|, \end{aligned} \quad (1)$$

where τ is the time-step size. The algorithm alternates between the oracle and the walk operators, yielding the time evolution

$$|\psi(\vec{x}; t_1, t_2)\rangle = [W^{t_1} R]^{t_2} |\psi(\vec{x}; 0, 0)\rangle. \quad (2)$$

Here t_2 is the number of oracle calls, and t_1 is the number of walk steps between the oracle calls. Both have to be optimized, depending on the spatial distribution of the vertices, to concentrate the amplitude distribution toward the marked vertex as quickly as possible and to solve the spatial search problem.

The iterative evolution of Eq.(2) redistributes the amplitude at each vertex over itself and its neighbors at every step. Unitarity of the evolution means that the eigenvalues have unit magnitude, and so the results of the algorithm are periodic in time. Grover's algorithm is the special case where one can move from any vertex to any other vertex in just one step, which can be interpreted as the $d \rightarrow \infty$ limit of spatial search [6]. Unlike Grover's algorithm, the maximum probability of being at the marked vertex, P , does not reach the value 1 for a generic spatial search. Augmenting the algorithm by the amplitude amplification procedure [11], the marked vertex can be found with probability $\Theta(1)$, and the overall complexity of the algorithm is then characterized by the effective number of oracle calls t_2/\sqrt{P} .

We have argued [6] that the spatial search in d dimensions obeys two lower bounds,

$$t_2 \geq \max\{dN^{1/d}, \pi\sqrt{N}/4\}. \quad (3)$$

They, respectively, follow from the distinct physical principles of special relativity (i.e. the walk must be able to travel across the lattice) and unitarity (i.e. Grover's algorithm is optimal in the absence of any constraint on walk

*Electronic address: adpatel@cts.iisc.ernet.in

†Electronic address: ksraghu@gmail.com

movements). The best spatial search algorithms, therefore, appear in the framework of relativistic quantum mechanics. Moreover, an analogy with statistical mechanics of critical phenomena in different dimensions, having an interplay of multiple dynamical features, provides an understanding of the scaling behavior of the spatial search. For $d > 2$, the latter bound wins, and the spatial search is $O(\sqrt{N})$ differing only in scaling prefactors. The two bounds cross in the critical dimension $d = 2$, where logarithmic corrections to scaling behavior are expected and have indeed been observed [2–5, 7]. For $d < 2$, the former bound dominates and should govern the scaling behavior of the spatial search. But the relativistic evolution operator is power-law infrared divergent there (as $\int d^d k/k^2$ in the continuum formulation), which may modify the scaling behavior compared to the bound.

The preceding arguments do not provide any new insight for $d = 1$, where both classical and quantum spatial search are $O(N)$. We need non-integral values of d to convincingly test the analogy of the spatial search with critical phenomena in statistical mechanics, and to that end we have investigated the spatial search on fractal lattices. Many candidates for fractal lattices are available with $1 < d < 2$, and for them we expect the spatial search to have a power-law scaling form, say $O(N^s)$. We want to determine how the exponent s depends on d , in particular whether it indeed equals $1/d$, and we specifically work with fractals known as Sierpinski gaskets.

II. QUANTUM WALK IN A FRACTAL GEOMETRY

Fractals are self-similar structures, and are conveniently defined using a recursive scheme in an embedding space, say of Euclidean dimensions $d_E > d$. (This is in contrast to regular lattices generated by repetitive unit cells in translationally invariant systems, where $d_E = d$.) For Sierpinski gaskets, the recursive structure is a regular simplex. That is an equilateral triangle for $d_E = 2$, and Fig. 1 illustrates the recursive generation of the Sierpinski gasket as a function of the stage number S .

At stage S , the linear extent of Sierpinski gaskets is $L = 2^S$. Since a simplex has $d_E + 1$ vertices, the total

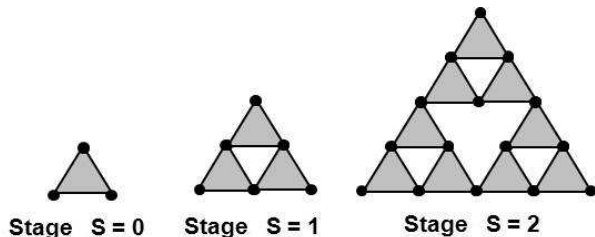


FIG. 1: Sierpinski gasket generation at various stages.

number of vertices N in Sierpinski gaskets is given by,

$$N(S) = \frac{(d_E + 1)((d_E + 1)^S + 1)}{2} \xrightarrow{S \rightarrow \infty} \left(\frac{d_E + 1}{2}\right) L^{\ln(d_E + 1)/\ln 2}. \quad (4)$$

Thus the fractal (also called the Hausdorff) dimension of Sierpinski gaskets is

$$d = \ln(d_E + 1)/\ln 2. \quad (5)$$

Dynamical phenomena on fractals have been investigated before [12, 13], in particular the classical random walk and the vibrational problem. Instead of the translational symmetry of regular lattices, self-similar fractals have the dilation (or the scale) symmetry. That leads to power-law scaling behavior for physical observables, and the critical exponents for various well-known fractals have been calculated. The most common operator appearing in the dynamical equations is the Laplacian, and the critical behavior is then governed by the scaling of its spectral density,

$$\rho(\omega) \sim \omega^{d_s - 1}. \quad (6)$$

This result can be understood as the reciprocal space for the Laplacian (or the Brillouin zone) having an effective dimension d_s , which is called the spectral (or the fracton) dimension [12, 13]. In the case of Sierpinski gaskets,

$$d_s = 2 \ln(d_E + 1)/\ln(d_E + 3), \quad (7)$$

which cannot exceed 2 although d can.

For regular lattices, $d_E = d = d_s$, whereas it is observed that $d_E \geq d \geq d_s$ in general. Note that both the position and the reciprocal space describe the same number of degrees of freedom in the same number of embedding dimensions. So $d \neq d_s$ means that the arrangement of vertices is different (in terms of connectivity as well as spacings) in the position and the reciprocal spaces. For the Sierpinski gaskets in two and three embedding dimensions, the relevant dimensions are:

$$\begin{aligned} d_E = 2 : & \quad d = 1.5849625 \dots, \quad d_s = 1.3652124 \dots, \\ d_E = 3 : & \quad d = 2, \quad d_s = 1.5474112 \dots. \end{aligned} \quad (8)$$

Both the classical random walk and the vibrational problem involve the same Laplacian in their spatial dependence, although they differ in their temporal dependence (first and second derivative respectively). So their critical exponents depend on the same d_s , but the dependence differs in phenomena involving temporal correlations. For the relativistic quantum walk problem we are addressing, the appropriate scaling behavior corresponds to that for the vibrational problem (and not the classical random walk).

Now quantum walk diffuses at relativistic speeds on a hypercubic lattice when the Dirac operator is used for time evolution. But it is unclear how to extend the relevant Clifford algebra to non-integer dimensions [14]. So

our earlier methodology for the spatial search on hypercubic lattices [3, 6, 7] cannot be implemented on fractals, and we need a different implementation of a quantum relativistic walk. It is known that the flip-flop walk diffuses relativistically [2], and can be easily applied to graphs where all the vertices have the same connectivity. That happens to be the case for Sierpinski gaskets, which have $2d_E$ neighbors for every vertex. We therefore first construct the flip-flop walk on Sierpinski gaskets, in terms of independent walk steps along every link, and then use it to study the spatial search problem.

III. THE FLIP-FLOP WALK

The flip-flop walk [2] is constructed in the joint Hilbert space containing both the position and the link degrees of freedom,

$$|\psi(\vec{x}, \hat{l})\rangle \equiv \sum_{x,l} a_{x,l} |\vec{x}\rangle \otimes |\hat{l}\rangle \in \mathcal{H}_N \otimes \mathcal{H}_k \equiv \mathcal{H}_{\text{search}}. \quad (9)$$

Every link attached to a given vertex is assigned its own direction pointing away from the vertex, so the dimension k of \mathcal{H}_k is the number of neighbors for the vertex. (For ease of implementation, we take this number to be the same for each vertex.) The walk step consists of a shift operation followed by a mixing of the link amplitudes, i.e. $W = GS$. The shift operation first propagates the quantum amplitude along its link direction, and then reverses the link direction,

$$|\vec{x}\rangle \otimes |\hat{l}\rangle \xrightarrow{S} |\vec{x} + \hat{l}\rangle \otimes |-\hat{l}\rangle. \quad (10)$$

Note that when the graph has a link \hat{l} at the vertex \vec{x} , it automatically has a link $-\hat{l}$ at the vertex $\vec{x} + \hat{l}$. The mixing of links at every vertex is the reflection in the mean operation (also referred to as the Grover coin [9]),

$$a_{x,l} \xrightarrow{G} \frac{2}{k} \sum_{l'} a_{x,l'} - a_{x,l}. \quad (11)$$

Both S and G are reflection operators, $S^2 = 1 = G^2$, and the walk spreads on the lattice because these two operators do not commute. S is block diagonal on the links, and its eigenstates are the combinations $|\vec{x}, \hat{l}\rangle \pm |\vec{x} + \hat{l}, -\hat{l}\rangle$ for every link, with eigenvalues ± 1 . Explicitly,

$$S = \bigoplus_{\text{links}} [(|\vec{x}, \hat{l}\rangle + |\vec{x} + \hat{l}, -\hat{l}\rangle) (\langle \vec{x}, \hat{l}| + \langle \vec{x} + \hat{l}, -\hat{l}|) - 1]. \quad (12)$$

On the other hand, G is block diagonal on the vertices,

$$G = \bigoplus_{\text{vertices}} \left[\frac{2}{k} \left(\sum_l |\vec{x}, \hat{l}\rangle \right) \left(\sum_{l'} \langle \vec{x}, \hat{l}'| \right) - 1 \right]. \quad (13)$$

For every vertex, it has one eigenvalue $+1$ corresponding to the isotropic distribution, and $k - 1$ eigenvalues -1 corresponding to other orthogonal distributions.

The unbiased uniform superposition state,

$$|s\rangle = (Nk)^{-1/2} \sum_{x,l} |\vec{x}, \hat{l}\rangle, \quad (14)$$

is invariant under both S and G (i.e. both operators have eigenvalue $+1$). Furthermore, the oracle R trivially commutes with G .

When the lattice has translational invariance, S can be simplified by Fourier transforming to the momentum space, and then the eigenspectrum of the walk can be obtained by diagonalizing a $k \times k$ matrix describing the operator W for each value of the momentum [2]. Such an analysis, however, is not possible for a fractal.

A. Flip-flop walk on Sierpinski gaskets

We first implement the flip-flop walk on the Sierpinski gasket in two dimensions. As can be seen from Fig. 1, all the internal vertices of the gasket have four neighbors, whereas the three corner vertices have only two neighbors. We increase the number of neighbors for the corner vertices to four, by providing a periodic wraparound as illustrated in Fig. 2. Furthermore, to conveniently label the vertices and to keep track of their neighbors, we embed the gasket in a two-dimensional rectangular grid as shown in Fig. 3.

In this configuration, there are six possible walk directions in general, as depicted in Fig. 4, out of which only four are valid for any given vertex. We separate the vertices into six types, also shown in Fig. 4, depending on which of the four walk directions are applicable to them. Note that V0, V1 and V2 are internal vertices, whereas V3, V4 and V5 are the corner vertices.

With this infrastructure, we can now explicitly write down the operations involved in the flip-flop walk. The

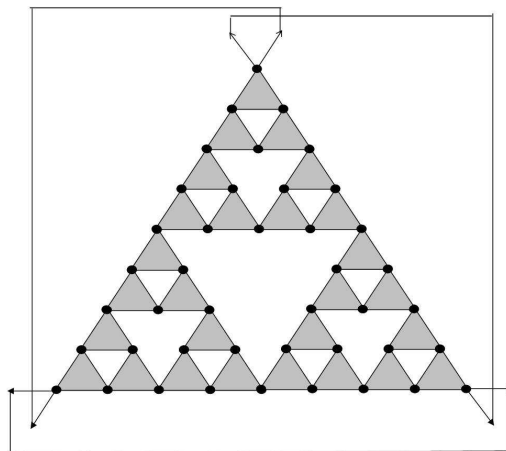


FIG. 2: Wraparound for the corner vertices of the two-dimensional Sierpinski gasket.

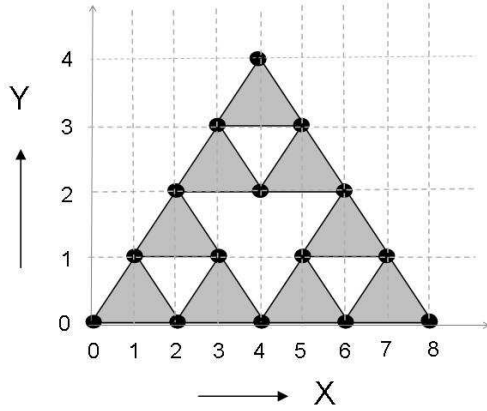


FIG. 3: Embedding of the two-dimensional Sierpinski gasket in a rectangular grid.

shift operation is:

$$\mathcal{S} = \begin{cases} |x, y\rangle \otimes |0\rangle \longleftrightarrow |x+2, y\rangle \otimes |3\rangle, \\ |x, y\rangle \otimes |1\rangle \longleftrightarrow |x+1, y+1\rangle \otimes |4\rangle, \\ |x, y\rangle \otimes |2\rangle \longleftrightarrow |x-1, y+1\rangle \otimes |5\rangle. \end{cases} \quad (15)$$

The mixing of link amplitudes occurs only among the four valid directions at each vertex. It can be described by the operator matrix,

$$G^{(k=4)} = 1 \otimes \frac{1}{2} \begin{pmatrix} -1 & 1 & 1 & 1 \\ 1 & -1 & 1 & 1 \\ 1 & 1 & -1 & 1 \\ 1 & 1 & 1 & -1 \end{pmatrix}. \quad (16)$$

These definitions can be easily extended for flip-flop walks on Sierpinski gaskets in any number of dimensions, with $k = 2d_E$.

B. Flip-flop walk as a relativistic propagator

To understand the time evolution provided by the flip-flop walk operator, we describe it for a hypercubic lattice in an integer number of dimensions, in a notation that identifies \mathcal{H}_k with internal degrees of freedom.

For $d = 1$, the shift operator is

$$\begin{aligned} \mathcal{S} &= \sum_x (1 \otimes \sigma_1) \\ &\times \left[|x+1\rangle \langle x| \otimes \frac{1+\sigma_3}{2} + |x-1\rangle \langle x| \otimes \frac{1-\sigma_3}{2} \right] \\ &= \sum_x \left[|x+1\rangle \langle x| \otimes \sigma_- + |x-1\rangle \langle x| \otimes \sigma_+ \right], \end{aligned} \quad (17)$$

and the link-mixing operator is $G^{(k=2)} = 1 \otimes \sigma_1$. Together they produce a directed walk, where the two spinor components propagate independently and at full speed in

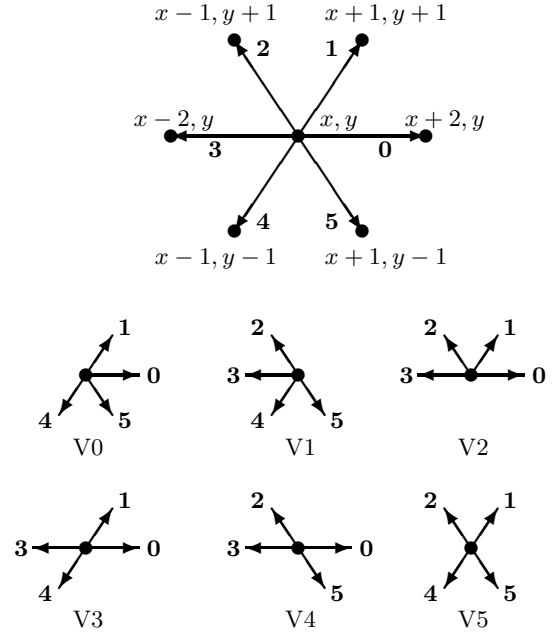


FIG. 4: Above: possible walk directions, and below: various vertex types, for the two-dimensional Sierpinski gasket.

opposite directions,

$$W = \sum_x \left[|x+1\rangle \langle x| \otimes \frac{1+\sigma_3}{2} + |x-1\rangle \langle x| \otimes \frac{1-\sigma_3}{2} \right]. \quad (18)$$

This is a representation of the massless Dirac propagator, in the basis where the two spinor components describe the two chiral degrees of freedom in $d = 1$. It is also the representation of the massless scalar Klein-Gordon propagator, where the two parts of the d'Alembert solution travel independently in opposite directions.

The situation in higher dimensions is more non-trivial. For a hypercubic lattice in d dimensions, size $L = N^{1/d}$ and connectivity $k = 2d$. The matrix $W = G\mathcal{S}$ is unitary, with eigenvalues of unit magnitude and orthogonal eigenvectors. Its spectrum can be obtained as follows. The momentum components on a periodic lattice are $k_i = 2\pi l_i/L$, with $l_i \in \{0, 1, \dots, L-1\}$. Select a specific set of momentum components $\{k_i\}$. Then pick any two-dimensional subspace, from the $(d-1)$ linearly independent choices $(x_1, x_2), (x_1, x_3), \dots, (x_1, x_d)$. In this subspace,

$$\mathcal{S} = \begin{pmatrix} 0 & e^{-ik_a} & 0 & 0 \\ e^{ik_a} & 0 & 0 & 0 \\ 0 & 0 & 0 & e^{-ik_b} \\ 0 & 0 & e^{ik_b} & 0 \end{pmatrix}, \quad (19)$$

and $G_{ij} = -\delta_{ij} + 1/d$. Corresponding to each direction, \mathcal{S} has eigenvalues $\lambda = \pm 1$ with eigenvectors $(1, \lambda e^{ik_a})$. From the degenerate pair of eigenvectors in every two-dimensional subspace, one can construct combinations that are orthogonal to $(1, 1, 1, 1)$. Acting on

these combinations, G reduces to $-I$, and so the combinations are eigenvectors of W with eigenvalues $-\lambda$. Explicitly, they are $(1 + \lambda e^{ik_b}, \lambda e^{ik_a}(1 + \lambda e^{ik_b}), -(1 + \lambda e^{ik_a}), -\lambda e^{ik_b}(1 + \lambda e^{ik_a}))$, with vanishing components outside the two-dimensional subspace. The $(d-1)$ linearly independent choices of two-dimensional subspaces thus yield $(d-1)$ -fold degenerate eigenvalues ± 1 for W . The remaining two eigenvalues of W are a complex conjugate pair $e^{\pm i\omega(k_i)}$, and $\text{Tr}(W)$ determines their real part as $\cos(\omega(k_i)) = \frac{1}{d} \sum_i \cos(k_i)$.

We observe that the ± 1 eigenvalues of the flip-flop walk correspond to local modes that can be restricted to two-dimensional subspaces, whereas the complex conjugate pair of eigenvalues provides relativistic propagation with speed $1/\sqrt{d}$. With this break up of the evolution modes, we can surmise that the flip-flop walk contains a single first-order form [15] of the complex massless Klein-Gordon operator, which makes its dynamics relativistic. The scalar Klein-Gordon operator can be mathematically constructed in any number of dimensions, even non-integer ones, unlike the spinor Dirac operator. Our simulation results in the next section demonstrate that the flip-flop walk indeed achieves the desired goals for the spatial search problem, and it would be interesting to explore its usefulness in other relativistic problems involving scalar fields in non-integer dimensions (or curved spaces).

IV. SPATIAL SEARCH USING THE FLIP-FLOP WALK

We first simulated the spatial search algorithm, for a single marked vertex on Sierpinski gaskets, as defined by Eq.(2). We chose the initial state to be the unbiased uniform superposition state, as is customary. Our numerical results are described later in the section. In particular, we needed $t_1 = 2$ for the search to succeed with reasonable probability ($t_1 = 1$ did not work as well, and $t_1 = 3$ was far worse), and both the success probability and the number of oracle calls showed power-law dependence on the database size N . Note that our spatial search algorithm is different from that of Ref.[2] for two reasons (although we use the same flip-flop walk): (i) we allow for values of $t_1 \neq 1$, and (ii) our oracle flips only the sign of the marked vertex amplitude, whereas Ref.[2] applies the link-mixing operator $G^{(k)}$ at the marked vertex together with the sign flip.

Since the flip-flop walk corresponds to a massless evolution propagator, this algorithm suffers from infrared divergence and is not optimal. Tulsi showed how to eliminate the infrared divergence of the spatial search algorithm by controlling the evolution operators using an ancilla qubit [4]. The ancilla control traps the quantum walk at the marked vertex and enhances the algorithm's success probability. Explicitly, in the joint space $\mathcal{H}_{\text{ancilla}} \otimes \mathcal{H}_{\text{search}}$, the $|1\rangle \otimes |\vec{x}, \hat{l}\rangle$ states are the original search space states, the $|0\rangle \otimes |\vec{x} = t, \hat{l}\rangle$ state is the new

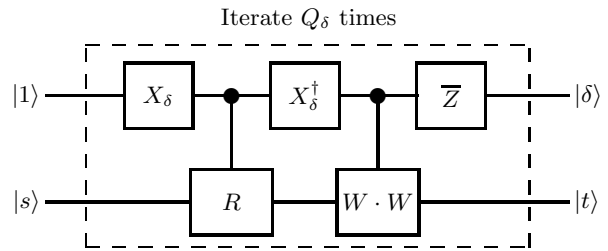


FIG. 5: Logic circuit diagram for Tulsi's controlled quantum spatial search algorithm. R and W are the binary oracle and the quantum walk operator respectively. We use the generalization with two walk steps after each oracle.

trap state that develops a nonzero amplitude, and the $|0\rangle \otimes |\vec{x} \neq t, \hat{l}\rangle$ states maintain zero amplitudes. This feature can be interpreted as the introduction of an effective mass at the marked vertex in the Hamiltonian [7], or as the introduction of a self-loop at the marked vertex in the graph [16]. Tulsi's scheme is illustrated in Fig. 5, where the ancilla operators are

$$X_\delta = \begin{pmatrix} \cos \delta & \sin \delta \\ -\sin \delta & \cos \delta \end{pmatrix}, \quad \bar{Z} = \begin{pmatrix} -1 & 0 \\ 0 & 1 \end{pmatrix}, \quad (20)$$

and the algorithm evolves the initial state $|1\rangle \otimes |s\rangle$ to the target state $|\delta\rangle \otimes |t, \hat{l}\rangle$ with $|\delta\rangle = X_\delta^\dagger |1\rangle$. Note that for the generic state corresponding to Eq.(9), the probability of being at the marked vertex is $\sum_l (|a_{\vec{x}=t, l}^{(0)}|^2 + |a_{\vec{x}=t, l}^{(1)}|^2)$, where the superscript refers to the ancilla value.

For $\delta = 0$, Tulsi's algorithm reduces to spatial search described by Eq.(2). It finds the marked vertex with probability $P_0 = \Theta(N^{-a})$ using $Q_0 = \Theta(N^b)$ oracle calls. Tulsi showed that, with $\cos \delta = \Theta(\sqrt{P_0})$, the algorithm increases the probability of finding the marked vertex to $P_\delta = \Theta(1)$ without changing the scaling of oracle calls $Q_\delta = \Theta(N^b)$ [4]. More explicitly, the algorithm largely confines the evolution of the quantum state to a two-dimensional subspace of \mathcal{H}_N , whereby

$$P_\delta = \frac{1}{B_\delta^2}, \quad Q_\delta = \frac{\pi B_\delta \sqrt{N}}{4 \cos \delta}, \quad (21)$$

$$B_\delta^2 = 1 + (B^2 - 1) \cos^2 \delta. \quad (22)$$

Here $B \equiv B_0 = \Theta(N^{a/2})$ is a second moment constructed from the eigenspectrum of W , and characterizes the infrared divergence of the problem. Also, Eq.(21) relates the scaling exponents,

$$a = 2b - 1. \quad (23)$$

The optimal value of the ancilla control parameter is obtained by minimizing the algorithmic complexity,

$$(\cos \delta)_{\text{opt}} = (B^2 - 1)^{-1/2} \approx 1/B, \quad (B_\delta^2)_{\text{opt}} = 2, \quad (24)$$

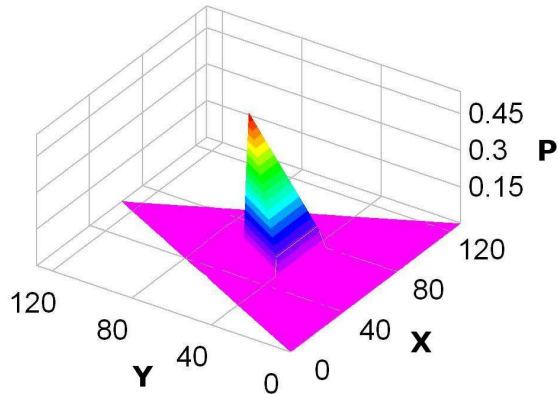


FIG. 6: (Color online) A snapshot of the probability distribution for the spatial search on the two-dimensional Sierpinski gasket, when the marked vertex attains its peak probability. The data are for $S = 6$ with ancilla control.

$$\left(\frac{Q_\delta}{\sqrt{P_\delta}}\right)_{\min} = \frac{\pi\sqrt{N}B}{2} = \Theta(N^b). \quad (25)$$

In what follows, we check these expectations regarding the scaling behavior of the spatial search, for Sierpinski gaskets in two and three dimensions.

A. Simulation results for $d_E = 2$

We simulated the spatial search algorithm on the two-dimensional Sierpinski gasket, for stage $S = 4 - 14$ corresponding to $N = 123 - 7174455$. To keep the memory requirements under control, we kept track of the irregular pattern of vertices and their neighbors using hash tables. We first checked that the algorithm did produce an approximately periodic evolution for the probability at the marked vertex, and the probability peak was reasonably sharp for the parameters we chose. For $S = 6$ ($N = 1095$) and the marked vertex in the center of the gasket, a snapshot of the probability distribution is presented in Fig. 6, and the probability evolution at the marked vertex is shown in Fig. 7. We find that the probability evolution is smoother with ancilla control than without it, implying that ancilla control improves the confinement of the evolution of the quantum state to a two-dimensional subspace of \mathcal{H}_N .

Implementing the spatial search algorithm without ancilla control was quite straightforward. But to implement Tulsi's algorithm, we needed the optimal value of $\cos\delta$, and we did not have any analytical estimate for it. So we just assumed Eqs.(21) and (24) to be valid, and extracted $(\cos\delta)_{\text{opt}}$ from the result for P_0 at each stage S . That worked well, and we obtained $P_\delta \approx 0.5$ as predicted.

Lack of translational invariance for a fractal means that the spatial search results depend on the location of the marked vertex. In the absence of ancilla control, each of Q_0 , P_0 and $Q_0/\sqrt{P_0}$ showed variation up to a factor of 2.2, as we moved around the position of the marked

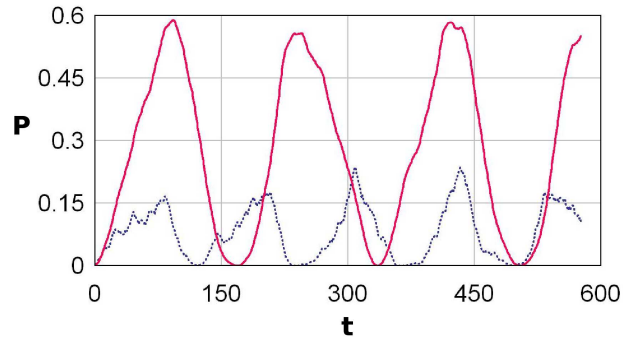


FIG. 7: (Color online) Time evolution of the marked vertex probability for the spatial search on the two-dimensional Sierpinski gasket. The data are for $S = 6$. Those without ancilla control are shown as the dotted curve, and those with ancilla control are shown as the continuous curve.

vertex in the gasket. With ancilla control, variation in Q_δ was somewhat smaller, up to a factor of 1.6, whereas $P_\delta \approx 0.5$ remained valid (within 10%) everywhere as expected. We also observed that the largest variation in the spatial search results was between the marked vertex positions at the corner and the center of the gasket. More importantly, when we extracted the scaling behavior from our results, holding the relative position of the marked vertex in the gasket (i.e. \bar{x}/L) fixed, we found that the variation was essentially in the prefactors and the scaling exponents changed by less than a percent. Henceforth we opted to keep the marked vertex at the center of the gasket, and all our results that follow correspond to that choice.

Our data for the number of oracle calls Q and the corresponding peak probability P are presented in Figs. 8 and 9, both without and with ancilla control. The figures also show simple scaling fits that were performed in the range $S = 8 - 14$.

In the absence of ancilla control, our fits give:

$$\begin{aligned} \log_2 Q_0 &= -1.066 + 0.730 \log_2 N \quad (\text{err} = 0.004), \\ \log_2 P_0 &= 1.995 - 0.440 \log_2 N \quad (\text{err} = 0.030). \end{aligned} \quad (26)$$

Here “err” refers to the r.m.s. deviation in the data from the fit. The dominant error in the asymptotic scaling parameters is the systematic error due to finite values of N . So we quote as our error estimates, the difference in the numbers for fits corresponding to $S = 7 - 14$ and $S = 8 - 14$. Then the results of Eq.(26) translate to the scaling behavior:

$$\begin{aligned} Q_0 &= 0.478(13) N^{0.730(2)}, \\ P_0 &= 3.99(20) N^{-0.440(4)}. \end{aligned} \quad (27)$$

The scaling exponents satisfy the relation Eq.(23) well, which supports Tulsi's analysis criterion that the quantum state evolution is largely confined to a two-dimensional subspace of \mathcal{H}_N .

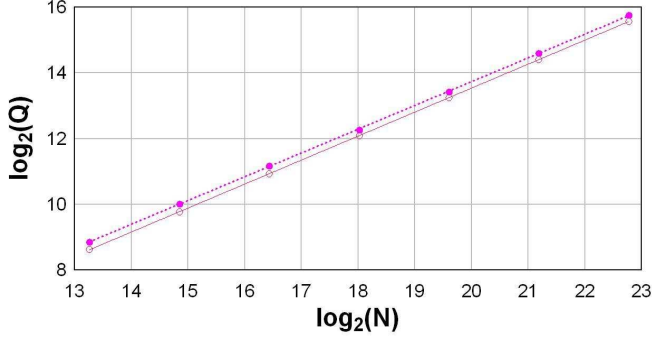


FIG. 8: (Color online) Scaling of the number of oracle calls for the spatial search on the two-dimensional Sierpinski gasket. The open and filled symbols denote data without and with ancilla control respectively. The linear fits are for the data from $S = 8$ to $S = 14$.

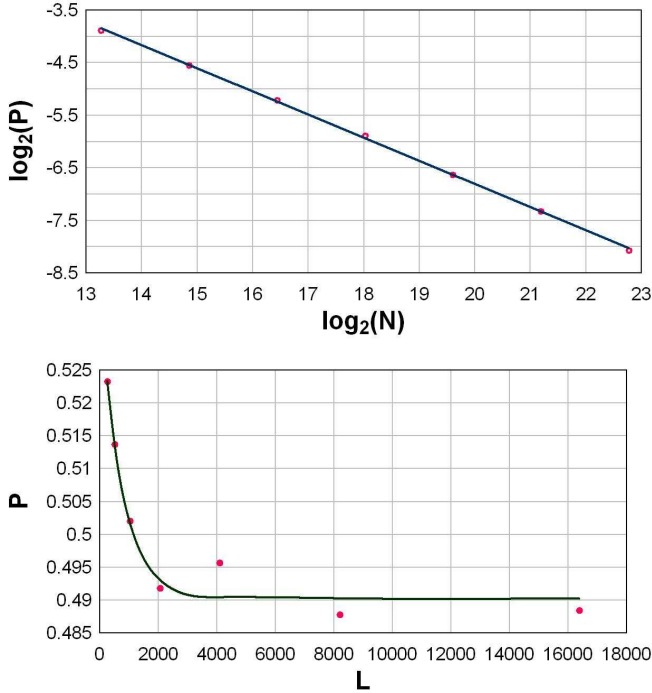


FIG. 9: (Color online) Scaling of the peak probability for the spatial search on the two-dimensional Sierpinski gasket, without (top) and with (bottom) ancilla control. The fits are for the data from $S = 8$ to $S = 14$, linear (top) and exponential (bottom) respectively.

The fits for our results with ancilla control, with $\cos \delta$ determined from the value of P_0 , give:

$$\begin{aligned} \log_2 Q_\delta &= -0.739 + 0.724 \log_2 N \quad (err = 0.017), \quad (28) \\ P_\delta &= 0.4903 + 0.0471 e^{-0.00137L} \quad (err = 0.0023). \end{aligned}$$

As displayed in Fig. 8, Q_δ is only marginally higher than Q_0 , and the scaling exponent b is essentially unchanged. On the other hand, Fig. 9 shows that P_δ approaches a

constant close to 0.5. Both these features fully agree with Tuli's predictions. We estimate the scaling behavior as:

$$Q_\delta = 0.599(8) N^{0.724(1)}, \quad P_\delta = 0.4903(2). \quad (29)$$

Also, direct fits for the complexity behavior give:

$$\begin{aligned} \log_2(Q_\delta/\sqrt{P_\delta}) &= -0.334 + 0.729 \log_2 N \quad (err = 0.015), \\ Q_\delta/\sqrt{P_\delta} &= 0.794(13) N^{0.729(1)}. \quad (30) \end{aligned}$$

We observe that the exponent $b \approx \frac{1}{d_s} = 0.73248676 \dots$ That clearly obeys the bound in Eq.(3), since $1/d \leq 1/d_s$. But more than that, our results imply that, for a fractal, the relevant length scale for the spatial search is not its linear extent $L \sim N^{1/d}$, rather it is the inverse of the linear extent of its reciprocal space N^{1/d_s} . Thus it is the smaller spectral dimension which governs the dynamics of the search process on fractals.

B. Simulation results for $d_E = 3$

To reinforce our observations, we extended our simulations of the spatial search algorithm to the three-dimensional Sierpinski gasket. In this case, the recursive structure is a tetrahedron, whereas the linear extent at stage S remains $L = 2^S$. Each internal vertex of the gasket now has six neighbors, and every corner vertex has a periodic wraparound with the other three corner vertices. Furthermore, there are twelve possible walk directions in general, out of which only six are valid at any given vertex. In our explicit operations, we used six types of internal vertices, four types of corner vertices, and the link-mixing operator $G^{(k=6)}$.

We obtained results for stage $S = 3 - 10$ corresponding to $N = 130 - 2097154$, and the marked vertex at the center of the gasket. Although not as extensive as the results for the $d_E = 2$ case, these are sufficient to discern the patterns in the scaling laws.

We again first simulated the algorithm without ancilla control, and then used $(\cos \delta)_{\text{opt}}$ extracted from the value of P_0 for each stage S to simulate the algorithm with ancilla control. Our results are plotted in Figs. 10 and 11, together with the simple scaling fits that were performed in the range $S = 5 - 10$. Without ancilla control, our fits give:

$$\begin{aligned} \log_2 Q_0 &= -0.767 + 0.641 \log_2 N \quad (err = 0.002), \\ \log_2 P_0 &= 1.39 - 0.265 \log_2 N \quad (err = 0.036). \quad (31) \end{aligned}$$

Again, “*err*” refers to the r.m.s. deviation in the data from the fit. For the error estimates on the fit parameters, we quote the difference in the numbers for fits corresponding to $S = 5 - 10$ and $S = 6 - 10$. Then the corresponding estimates of the scaling behavior are:

$$\begin{aligned} Q_0 &= 0.588(1) N^{0.641(1)}, \\ P_0 &= 2.62(25) N^{-0.265(7)}. \quad (32) \end{aligned}$$

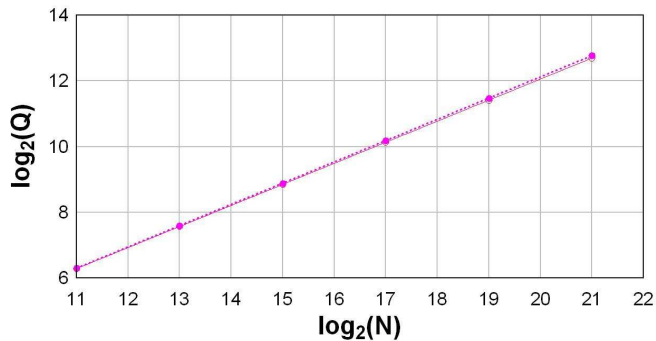


FIG. 10: (Color online) Scaling of the number of oracle calls for the spatial search on the three-dimensional Sierpinski gasket. The open and filled symbols denote data without and with ancilla control respectively. The linear fits are for the data from $S = 5$ to $S = 10$.

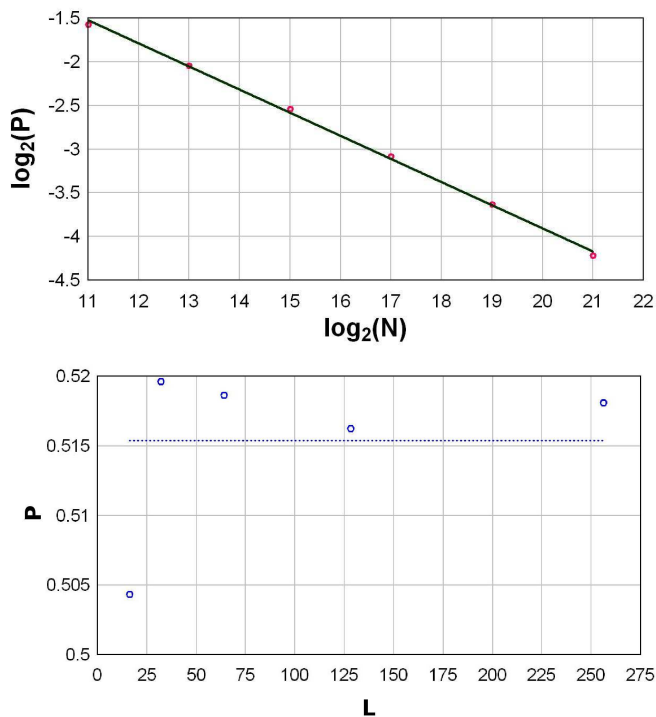


FIG. 11: (Color online) Scaling of the peak probability for the spatial search on the three-dimensional Sierpinski gasket, without (top) and with (bottom) ancilla control. The fits are for the data from $S = 5$ to $S = 10$, linear (top) and constant (bottom) respectively.

Once more, the scaling exponents reasonably satisfy the relation Eq.(23), and $b \approx \frac{1}{d_s} = 0.64624063\dots$

With ancilla control, our fits yield:

$$\log_2 Q_\delta = -0.817 + 0.647 \log_2 N \quad (err = 0.003),$$

$$P_\delta = 0.518 \quad (err = 0.001). \quad (33)$$

We observe that Q_δ is only slightly larger than Q_0 , the scaling exponent b is essentially the same, and P_δ is a constant close to 0.5, all consistent with Tulsi's predictions. We estimate the scaling behavior as:

$$Q_\delta = 0.568(4) N^{0.647(1)}, \quad P_\delta = 0.518(1). \quad (34)$$

Moreover, direct fits for the complexity behavior give:

$$\begin{aligned} \log_2(Q_\delta/\sqrt{P_\delta}) &= -0.343 + 0.647 \log_2 N \quad (err = 0.002), \\ Q_\delta/\sqrt{P_\delta} &= 0.788(3) N^{0.647(1)}. \end{aligned} \quad (35)$$

Here the fact that $b \approx \frac{1}{d_s}$ is an important finding. In this case, the embedding dimension $d_E = 3$ and the Hausdorff dimension $d = 2$. Were either of them controlling the scaling behavior of the spatial search, we would have found $Q = O(\sqrt{N})$. Our clearly distinct result once again tells us that the dynamics of the spatial search is governed by the spectral dimension.

V. CONCLUSION

We have described how the flip-flop walk contains within it a relativistic Klein-Gordon propagator, and then used it to solve the spatial search problem on fractals. The analogy with critical phenomena in statistical mechanics suggests that, for $1 < d < 2$, physical observables have power-law scaling behavior. Also, for $d \leq 2$, the fully relativistic spatial search algorithm suffers from infrared divergence, which we have suppressed by Tulsi's ancilla controlled version that is equivalent to the introduction of an effective mass or a self-loop at the marked vertex.

Specifically, we have carried out numerical simulations for Sierpinski gaskets in two and three dimensions, keeping the relative position of the marked vertex in the gasket fixed, and our results support all the expectations. An important finding is that we are able to reach the lower bound of $N^{1/d}$ oracle calls, where d is the spectral dimension and not the fractal dimension. These two dimensions are not equal for fractals, and we find that the smaller spectral dimension governs the scaling exponents. Note that the solution of the quantum spatial search problem has to be simultaneous in both the position space and the reciprocal momentum space. The position space evolution proceeds from a uniform distribution toward a δ -function, and the momentum space evolution proceeds from a δ -function toward a uniform distribution. Thus it is fully understandable that the stricter of the lower bounds (i.e. the smaller value of d_s) governs the scaling behavior of the problem.

-
- [1] N. Shenvi, J. Kempe and K.B. Whaley, Phys. Rev. A 67 (2003) 052307, arXiv:quant-ph/0210064.
- [2] A. Ambainis, J. Kempe and A. Rivosh, Proceedings of the Sixteenth Annual ACM-SIAM Symposium on Discrete Algorithms (SODA'05), (SIAM, Philadelphia, 2005), p. 1099, arXiv:quant-ph/0402107.
- [3] A. Patel, K.S. Raghunathan and P. Rungta, Proceedings of the Workshop on Quantum Information, Computation and Communication (QICC-2005), IIT Kharagpur, India (Allied Publishers, 2006), p. 41, arXiv:quant-ph/0506221.
- [4] A. Tuli, Phys. Rev. A 78 (2008) 012310, arXiv:0801.0497; see also Ph.D. thesis, Indian Institute of Science (2009).
- [5] G. Abal, R. Donangelo, F.L. Marquezino and R. Portugal, Math. Struct. Comp. Sci. 20 (2010) 999, arXiv:1001.1139.
- [6] A. Patel and M.A. Rahaman, Phys. Rev. A 82 (2010) 032330, arXiv:1003.0065.
- [7] A. Patel, K.S. Raghunathan and M.A. Rahaman, Phys. Rev. A 82 (2010) 032331, arXiv:1003.5564.
- [8] Y. Aharonov, L. Davidovich and N. Zagury, Phys. Rev. A 48 (1993) 1687.
- [9] J. Kempe, Contemporary Physics 44 (2003) 307, arXiv:quant-ph/0303081.
- [10] L.K. Grover, Pramana 56 (2001) 333, arXiv:quant-ph/0109116.
- [11] G. Brassard, P. Høyer, M. Mosca and A. Tapp, in *Quantum Computation and Information*, AMS Contemporary Mathematics Series Vol. 305, eds. S.J. Lomonaco and H.E. Brandt (AMS, Providence, 2002), p. 53, arXiv:quant-ph/0005055.
- [12] S. Alexander and R. Orbach, J. Phys. Lett. 43 (1982) 625.
- [13] R. Rammal and G. Toulouse, J. Phys. Lett. 44 (1983) 13.
- [14] Note that the Clifford algebra cannot be formulated in curved spaces either. Inclusion of fermions in general relativity needs vielbeins, with one index in the curved space and the other in the flat tangent space. The Dirac operator structure is defined in the flat tangent space, and is contracted with curved space variables using the vielbeins.
- [15] A second-order differential equation can always be rewritten as two coupled first-order differential equations, e.g. $\ddot{\psi} + \psi = 0$ and $\frac{d}{dt} \begin{pmatrix} \psi \\ \dot{\psi} \end{pmatrix} = \begin{pmatrix} 0 & 1 \\ -1 & 0 \end{pmatrix} \begin{pmatrix} \psi \\ \dot{\psi} \end{pmatrix}$ are equivalent descriptions of a scalar wave equation.
- [16] H. Krovi, F. Magniez, M. Ozols and J. Roland, Proceedings of the 37th International Colloquium on Automata, Languages and Programming (ICALP 2010), Lecture Notes in Computer Science Vol. 6198 (Springer, Berlin, 2010), p. 540, arXiv:1002.2419.